Experimental investigation of the influence of internal defects (voids, wrinkles) on the shear properties of CFRP

S.V. Slovikov
Center of Experimental Mechanics, Perm National Research Polytechnic University, Russia
sslovikov@ya.ru, https://orcid.org/0000-0003-3884-3882

D.S. Lobanov
Center of Experimental Mechanics, Perm National Research Polytechnic University, Russia
cem.lobanov@gmail.com, https://orcid.org/0000-0003-1948-436X

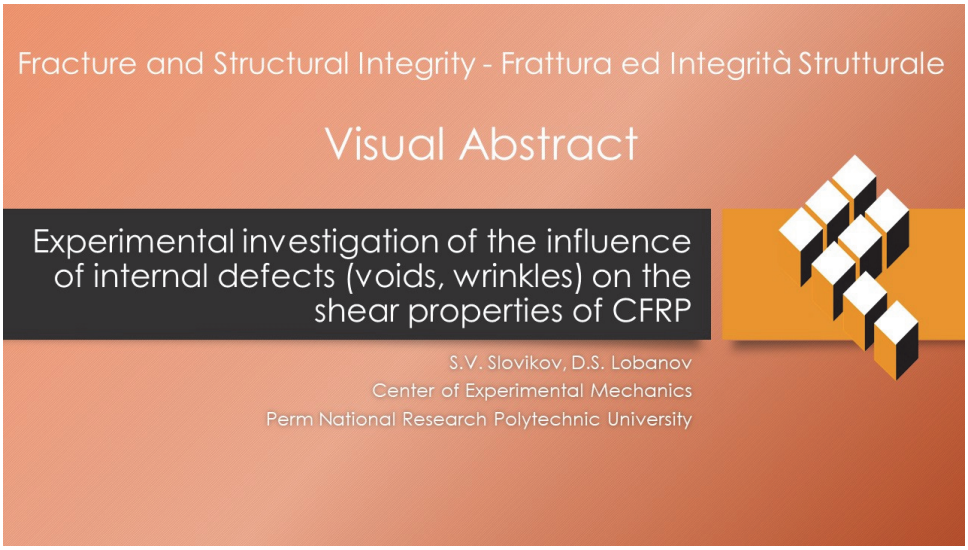

Citation: Slovikov, S.V.., Lobanov, D.S., Experimental investigation of the influence of internal defects (voids, wrinkles) on the shear properties of CFRP, Fracture and Structural Integrity, 75 (2026) 46-54.

Received: 07.07.2025
Accepted: 10.10.2025
Published: 16.10.2025
Issue: 01.2026

KEYWORDS. Carbon fiber reinforced polymer (CFRP), Shear, Voids, Wrinkles, Mechanical properties, Manufacturing defects.

INTRODUCTION

Carbon fiber reinforced polymers (CFRP) are key polymer matrix composites (PMCs) widely used in aerospace, automotive, and energy industries due to their high specific strength and stiffness [1–3]. However, CFRP's layered structure makes it vulnerable to internal process-induced defects during manufacturing. Common defects include dry-spot (incomplete resin impregnation), leading to voids, and wrinkles (layer waviness) [4–7]. These defects critically impact the design and operation of safety-critical structures, as minor deviations can cause catastrophic failures. Specifically, defects reduce the load-bearing capacity of composites under shear loading, which dominates multi-component systems. However, most studies on CFRP mechanical behavior assume idealized conditions, neglecting defect influence [~~7,~~8].
This work investigates the effects of void and wrinkle defects on the shear properties of CFRP. Recent studies confirm that CFRP shear strength depends on fiber orientation, matrix properties, and interfacial adhesion [9, 10]. Under in-plane shear,

matrix failure predominates over fiber failure [11]. Dry-spot defects arise from insufficient resin impregnation [11–14], evolving into voids [15]. Such defects typically form during layup and curing. Additional void sources include entrapped air bubbles between layers. Depending on size and concentration, voids can significantly degrade PMC mechanical properties [16–18]. Wrinkles also frequently occur in CFRP manufacturing [19, 20].

Optical methods like digital image correlation (DIC) [21, 22] are increasingly used to assess deformations in materials and structures. DIC effectively captures strain localization in defect zones and is widely applied to analyze PMCs [23–25].

The object of the study comprises specimens made of structural carbon fiber reinforced polymer (CFRP) VKU based on the VSE1212 epoxy matrix with a $[0/90]_{10}$ layup configuration. Specimens were fabricated with artificially introduced defects: voids (circular and square) and wrinkles.

The research objectives are to evaluate in-plane shear properties—ultimate strength, elastic modulus, failure modes, and strain distribution in defect zones. This work continues previously published research on the influence of internal manufacturing defects on the mechanical performance, fatigue life, and deformation behavior of layered carbon fiber composites [5,6]. The scientific significance of the entire study lies in the comprehensive systematizing data on defect geometry's influence on CFRP mechanical behavior. Results can inform non-destructive testing, process optimization, and defect-inclusive mathematical models.

METHODOLOGY AND EXPERIMENT

Defect geometry influences stress distribution. For instance, sharp corners in square voids act as stress concentrators, accelerating failure. Specimens for shear testing, both without defects and with defects, were manufactured using VKU-60 prepreg (with carbon fiber produced by VIAM) and VSE1212 polymer matrix, with a lay-up sequence of $[0/90]_{10}$, according to standard autoclave molding technology.

To compare shear behavior, two void geometries—circle (Ø 20 mm) and square (20×20 mm)—were embedded centrally in specimens, each with a thickness of one 0.1-mm epoxy layer. A specimen schematic is shown in Fig. 1(a).

Three with no defect specimens (width between V-notches: 32 mm, thickness: 2±0.05 mm; labels: bd-01, bd-02, bd-03), three wrinkle-defect specimens (sm-01, sm-02, sm-03), and six void-defect specimens were tested. Voids were created using 0.1-mm-thick fluoroplastic film: three circular (Ø 20 mm; kr-01, kr-02, kr-03) and three squares (20×20 mm; kv-01, kv-02, kv-03), placed in the central layer. Defect configurations are shown in Fig. 1(b).

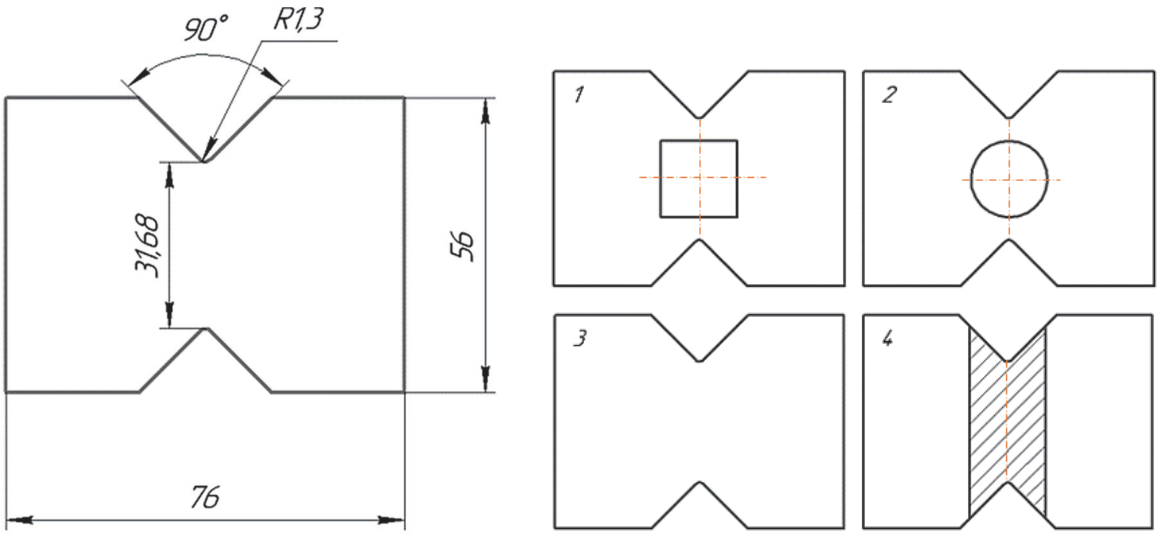

Figure 1: (a) Shear test specimen geometry; (b) Specimens with internal defects: 1 - square void, 2 - circular void, 3- no defect, 4 - wrinkle.

All defects were positioned between the 5th and 6th fiber layers. Void and wrinkle schematics are in Fig. 2.

Prior to testing, the specimens were examined using ultrasonic inspection on a TD FOCUS-SCAN RX, which revealed the absence of any defects within the specimen's working zone, except for the artificially introduced flaws shown in the Fig.2 subjected to testing.

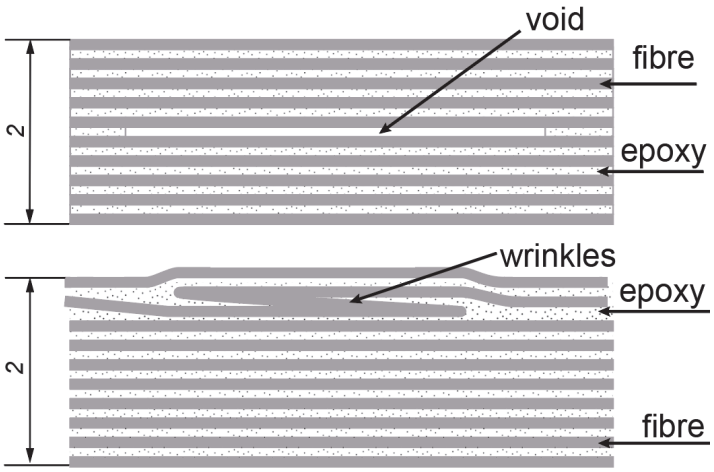

Figure 2: Void and wrinkle defects.

The test methodology according to ASTM D7078 assumes a hypothesis of pure shear up to 5% strain. Under this assumption, the object of investigation (specimen cross-section) is considered two-dimensional, and volume reduces to area. Therefore, for a two-dimensional object, the void concentration (area fraction) (k_v) is defined as the ratio of areas:

$$k_V = S_V / S \quad (1)$$

where S_V - cross-sectional area of the defect type void, S - cross-sectional area of the sample.
For voids, concentration (area fraction) (k_v) is 5.3%.
The wrinkles defect, a similar concentration (area fraction) estimate can be introduced:

$$k_W = S_W / S \quad (2)$$

where Sw - cross-sectional area of the defect type wrinkle.
For wrinkles k_W is 10.5%, which leads to an increase in the cross-sectional thickness in the working area of the wrinkle samples to 2.2±0.05 mm.
Tests were conducted at Perm National Research Polytechnic University's Experimental Mechanics Center. An Instron 5882 electromechanical system and Vic-3D DIC system were used. Specimen thickness (h) and width (d_i) were measured with a Mitutoyo 164-162 digital micrometer (resolution: 0.001 mm, accuracy: ±0.004 mm) and ShTsK-1-300-0.01 caliper (resolution: 0.01 mm, accuracy: ±0.04 mm). All instruments were certified.
Shear tests followed ASTM D7078 using precision Instron fixtures. Crosshead speed: 2 mm/min. Load was measured with a ±100 kN load cell (accuracy: 0.5% of the measured value). Vic-3D tracked displacement fields; a "virtual extensometer" module recorded strains by monitoring relative displacement between two surface points. Test setup and fixture are shown in Fig. 3.

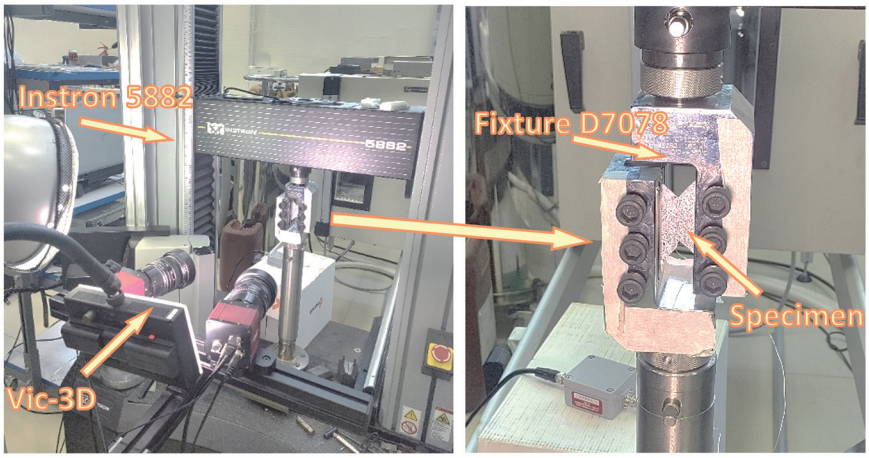

Figure 3: ASTM D7078 shear test setup.

The method involved relative motion of two grips, aligning V-notches with the load axis to induce shear stresses.

RESULTS

Per ASTM D7078, shear strength (MPa) and shear modulus (GPa) were determined. Mechanical properties are summarized in Tab. 1. Statistical processing of the results was performed in accordance with the recommendation in ASTM D7078, section 13.5, which suggests determining only the mean (average) and the coefficient of variation CV (in percent).

Defect Type	Specimen ID	Area, mm²	Load at 5% Strain, kN	Shear Strength (at 5%), MPa	Avg. Shear Strength, MPa	CV, %	Shear Modulus, GPa	Avg. Shear Modulus, GPa	CV, %
No defect	bd-01	67.3	4.79	71.3	72.1	1.7	4.34	4.49	3.6
	bd-02	65.9	4.85	73.5			4.45		
	bd-03	67.3	4.80	71.4			4.66		
Circular void	kr-01	67.3	4.76	70.8	70.5	2.1	4.37	4.48	6.9
	kr-02	67.9	4.88	71.8			4.83		
	kr-03	68.4	4.71	68.9			4.25		
Square void	kv-01	67.3	4.83	71.8	70.6	2.0	4.84	4.45	9.6
	kv-02	68.1	4.83	71.0			4.52		
	kv-03	68.1	4.70	69.1			3.99		
Wrinkles	sm-01	74.0	5.40	66.3	69.9	4.4	6.03	5.39	11.1
	sm-02	74.2	5.31	71.6			5.28		
	sm-03	73.6	5.28	71.7			4.85		

Table 1: Mechanical properties of CFRP specimens with and without defects

The shear modulus was determined in accordance with ASTM D7078, p. 13.3.1, using the chord method with a strain of 0.4%.

Shear stress-Shear strain (τ-γ) curves are in Fig. 4.

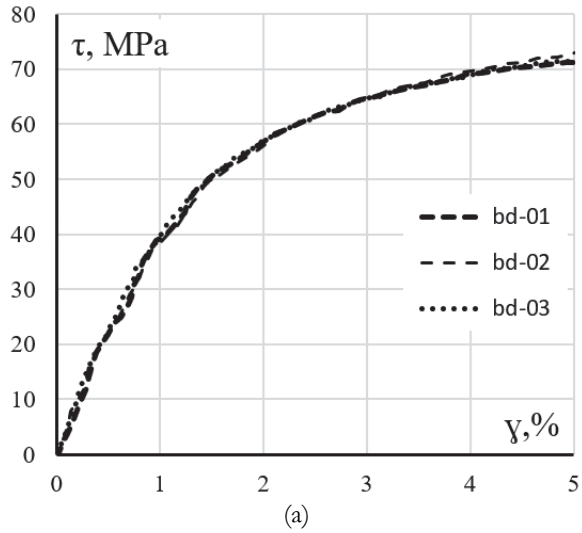

(a)

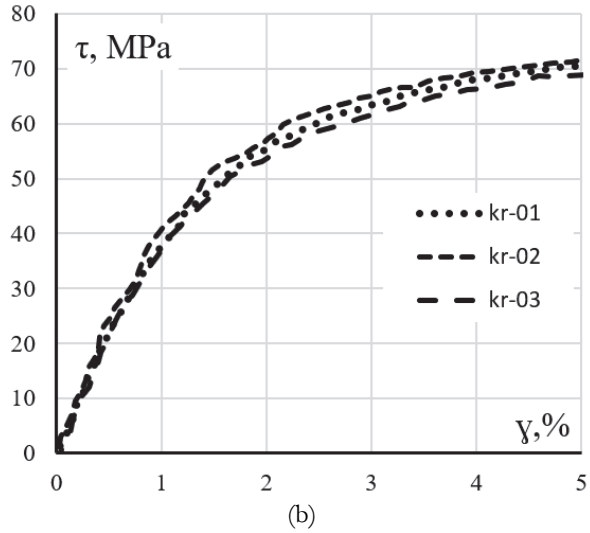

(b)

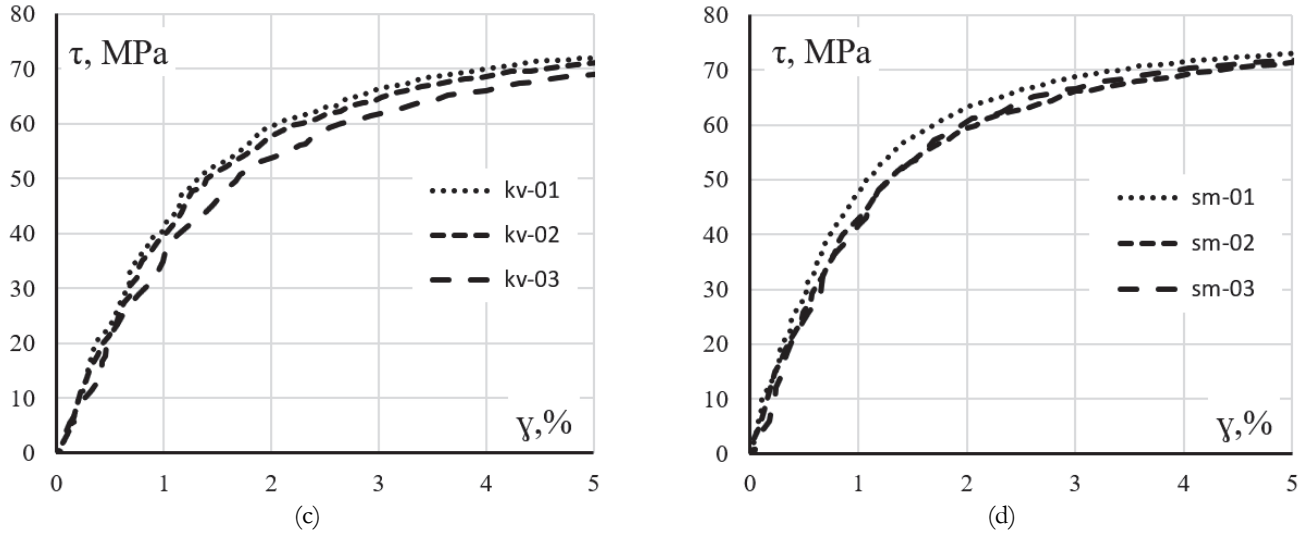

Figure 4: Shear stress (τ) vs. shear strain (γ) diagrams: (*a*) no Defect; (*b*) Square void (*c*); Circular void; (*d*) Wrinkles

Vic-3D data captured strain field evolution (ε_{xx}, ε_{yy}, ε_{xy}) at three load stages: initial, 5% strain, and peak load. Strain fields for no defects and wrinkle specimens are in Fig. 5; void specimens are in Fig. 6. Labels 1, 2, 3 denote load levels.

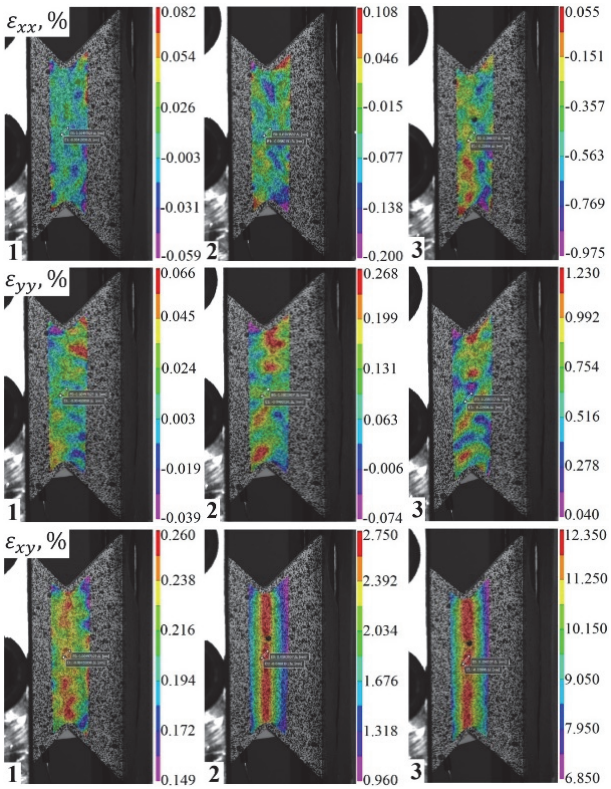

1-1.47 kN; 2- 4.80 kN; 3- 7.24 kN

a

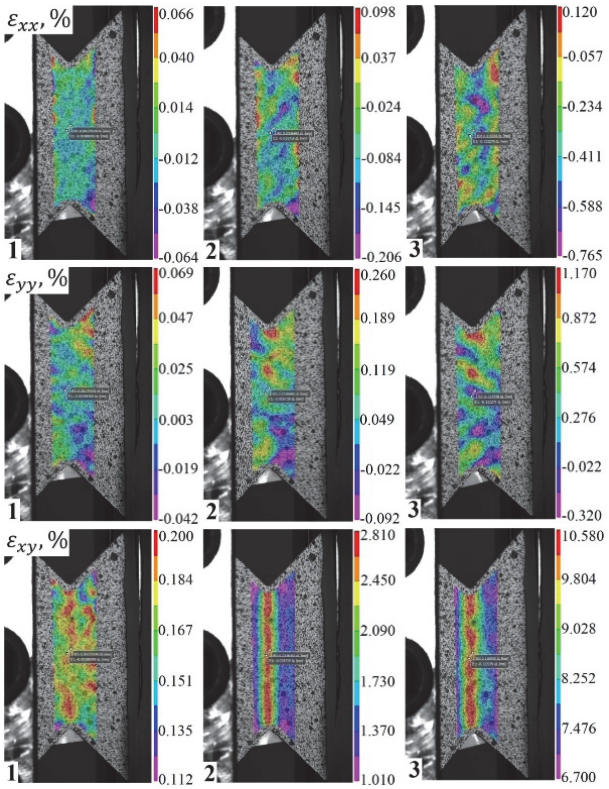

1-1.50 kN, 2 - 5.41 kN; 3- 7.67 kN

b

Figure 5: Strain field evolution: (*a*) no Defect; (*b*) Wrinkles.

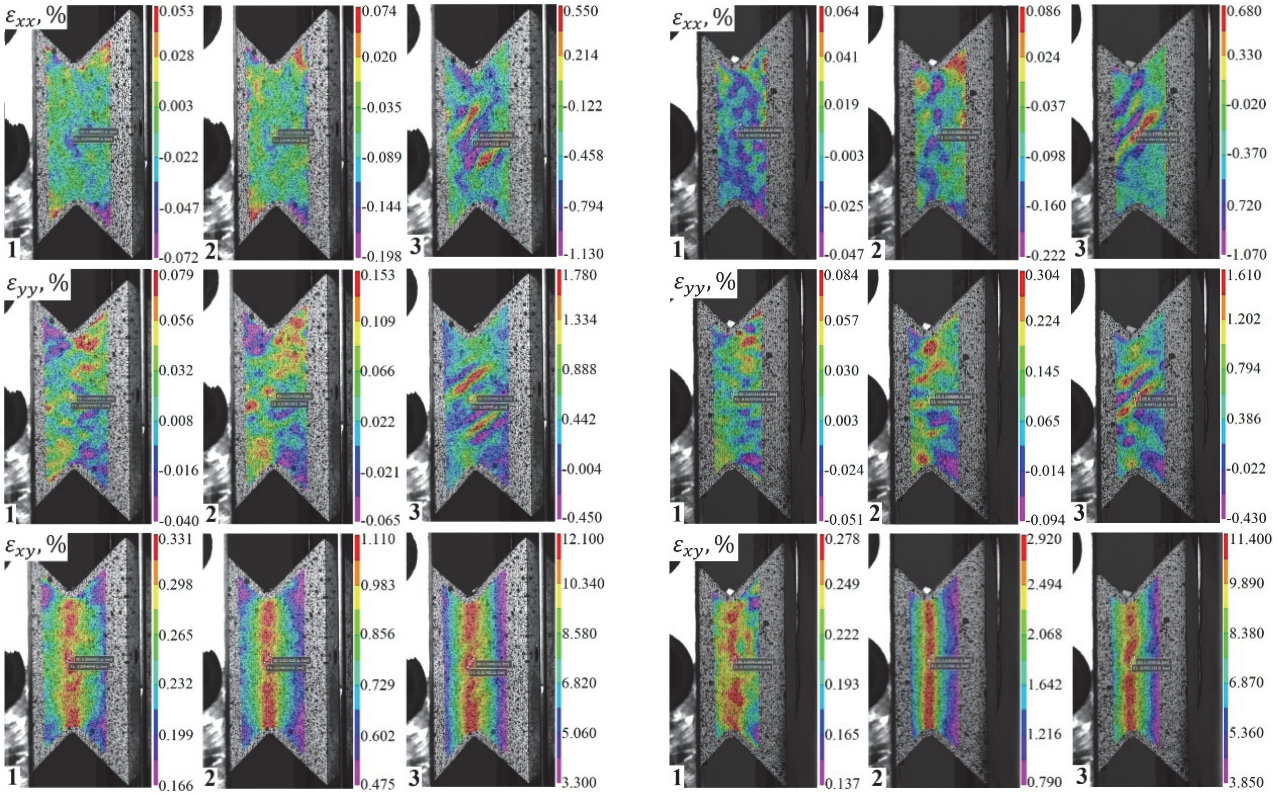

1.84 kN, 2- 3.88 kN; 3- 6.84 kN

a

1.58 kN; 2- 4.83 kN; 3- 6.67 kN

b

Figure 6: Strain field evolution: (*a*) Circular void; (*b*) Square void.

Discussion

Characteristic failure involved vertical cracks within the strain measurement zone between notches. According to the classification presented in ASTM D7078, the failure mode was classified as VGN (V: vertical cracking, G: Gage section, N: between Notches).

Stress-strain curves indicate minimal difference in shear modulus across specimen groups. Calculated data confirm this observation—low coefficient of variation (CV) values for each sample set demonstrate homogeneity.

Representative failure modes observed during testing are shown in Fig. 7.

Figure 7: Typical failure modes.

After the tests, the failed samples were analyzed, and the failure modes were classified for each sample in accordance with ASTM D7078 (Tab. 2).

Defect Type	Specimen ID	Types of destruction	Defect Type	Specimen ID	Types of destruction
No defect	bd-01	VGN	Square void	kv-01	VGN
	bd-02	VGN		kv-02	VGN
	bd-03	VGN		kv-03	VGN
Circular void	kr-01	VGN	Wrinkles	sm-01	VGN
	kr-02	VGN		sm-02	VGN
	kr-03	VGN		sm-03	VGN

Table 2: Classification of failure modes of carbon fiber reinforced plastic specimens after shear tests in accordance with ASTM D 7078.

It is worth noting that the typical failure mode observed in all tested samples was the formation of vertical cracks in the deformation measurement zone between the notches (designated as VGN). The absence of end-face crushing and slippage in the gripping fixtures indicates that the testing procedure was properly conducted and that the failure mode is valid. According to ASTM D7078, the VGN failure mode is considered acceptable. Therefore, all 12 samples exhibited VGN - type failure. Examples of sample failure during testing are shown in Fig. 8.

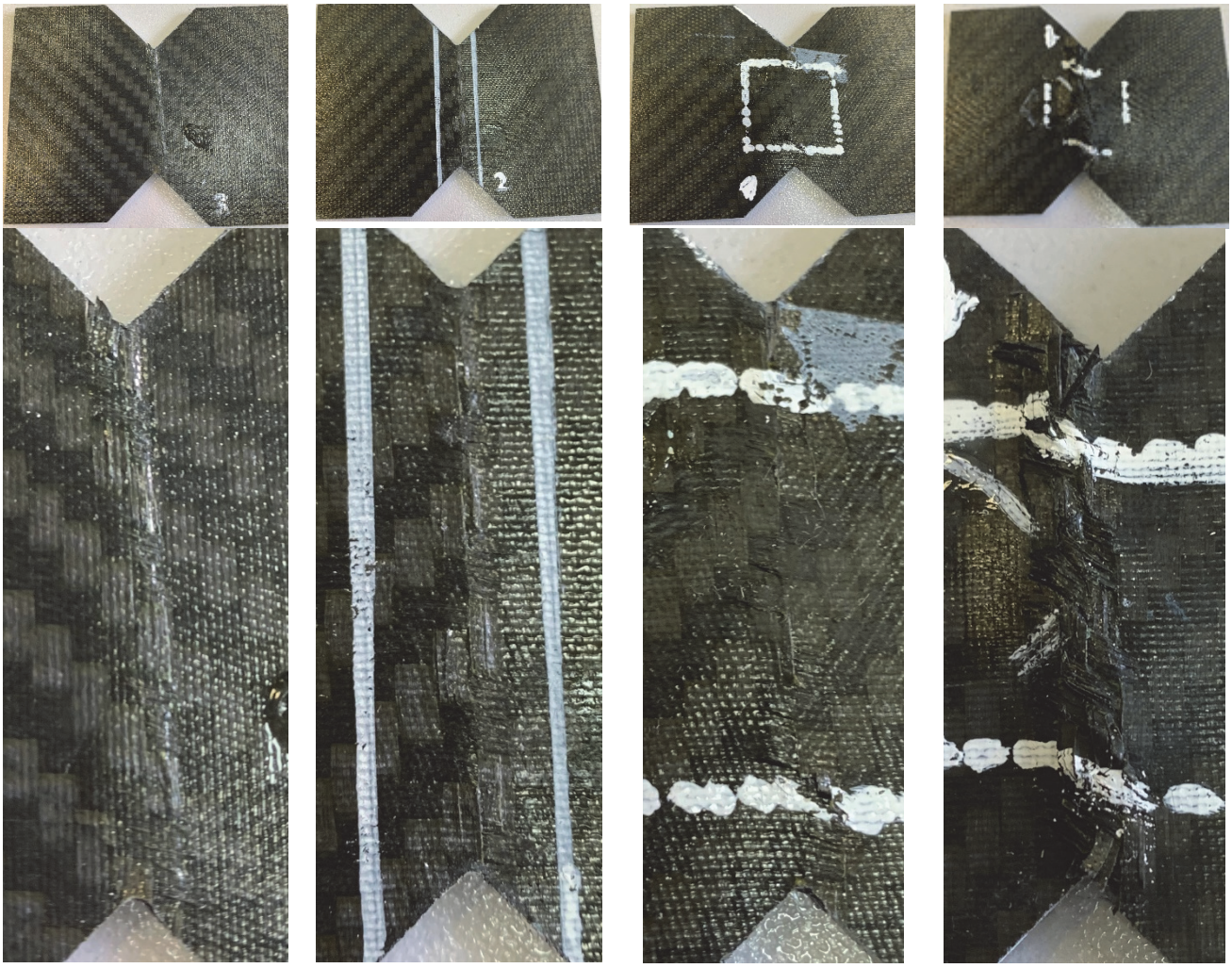

a *b* *c* *d*

Figure 8: Characteristic failure of samples: (*a*) no Defect; (*b*) Wrinkles; (*c*) Square void (*d*) Circular void.

Voids at 5.3% concentration (area fraction) reduced shear strength by 2.2% but had negligible impact on shear modulus (4.49 GPa → 4.45 GPa). Variability in modulus may stem from V-notch quality.
Wrinkle specimens (10% thicker, 12 vs. 10 layers) showed higher shear modulus (5.39 GPa) due to added layers. Shear strength decreased by ~3% (69.9 MPa vs. 72.1 MPa), indicating that localized fiber wrinkles did not critically weaken shear resistance.
The strain graphs (Fig. 4) show that the average shear modulus of the samples in each group differs only slightly, allowing a preliminary conclusion (due to the small number of tested samples) that the presence of internal defects such as wrinkles and voids with this volume fraction does not have a significant influence.

CONCLUSIONS

The study of the mechanical behavior of carbon fiber-reinforced polymer (CFRP) specimens with artificial defects (voids and wrinkles) under shear loading revealed key patterns. A void content of approximately 5.3%, regardless of void geometry (circular or square), reduced the average shear strength by 2.2% compared to no defect specimens. However, the defect geometry (presence of sharp corners in square-shaped voids) did not exert a significant effect on strength, underscoring the dominant influence of the defect area in governing the failure response under the specified shear loading conditions.
The shear modulus of specimens with voids (~4.48 GPa) was nearly identical to that of no defect specimens (~4.49 GPa), demonstrating minimal influence of such defects on elastic shear properties.
The failure mode of all specimens was consistent, characterized by vertical crack formation in the gauge region between V-shaped notches. Digital image correlation (DIC) analysis confirmed its effectiveness in tracking strain localization during deformation.
Findings indicate that moderate void content (~5%) causes a small reduction in the average shear strength. Similarly, localized wrinkles without material separation slightly reduce shear strength while increasing stiffness through thickness enhancement. However, due to the small number of tested specimens, this effect should be regarded only as a trend requiring further confirmation through additional testing. These results may have practical relevance for refining defect tolerance criteria in shear-loaded critical components, improving non-destructive testing methods, optimizing CFRP manufacturing processes to minimize critical defects, and validating mathematical models of composite strength and failure incorporating internal process-induced flaws.
Future research should focus on the combined effects of multiple defect types and the development of failure prediction criteria accounting for their spatial distribution and scale. The outcomes are also valuable for advancing digital twin methodologies in aerospace and energy sectors, where the reliability of layered composites under operational loads is critical.

ACKNOWLEDGEMENTS

This research was funded by the Ministry of Science and Higher Education of the Russian Federation (Project № FSNM-2024-0013).

REFERENCES

[1] Li, H., Fiore, L., Jiang, Z. (2020). Composite materials for primary aircraft structures: from development phase to high volume production rate, Civ. Aircr. Des. Res., (1), pp. 125–128. DOI: https://doi.org/10.19416/j.cnki.1674-9804.2020.01.021.
[2] Kormanikova, E., Zmindak, M., Novak, P., Sabol, P. (2021). Tensile properties of carbon fiber reinforced polymer matrix composites: Application for the strengthening of reinforced concrete structure, Compos. Struct., 275, p. 114448. DOI: https://doi.org/10.1016/j.compstruct.2021.114448.
[3] Lee, J.-M., Lee, C.-J., Kim, B.-M., Ko, D.-C. (2020). Design of Prepreg Compression Molding for Manufacturing of CFRTP B-pillar Reinforcement with Equivalent Mechanical Properties to Existing Steel Part, Int. J. Precis. Eng. Manuf., 21(3), pp. 545–556. DOI: https://doi.org/10.1007/s12541-019-00265-z.
[4] Heslehurst, R.B. (2014). Defects and Damage in Composite Materials and Structures, 0 ed., CRC Press,

DOI: https://doi.org/10.1201/b16765.
[5] Lobanov, D., Slovikov, S., Lunegova, E. (2023). Influence of Internal Technological Defects on the Mechanical Properties of Structural CFRP, Frat. Ed Integrità Strutt., 17, pp. 74–87. DOI: https://doi.org/10.3221/IGF-ESIS.65.06.
[6] Slovikov, S., Lobanov, D.S., Chebotareva, E., Melnikova, V. (2024). The influence of technological defects on the mechanical behavior of CFRP during buckling under compression based on DIC data and acoustic emission, Fract. Struct. Integr., 18(69), pp. 60–70. DOI: https://doi.org/10.3221/IGF-ESIS.69.05.
[7] Lobanov D.S., Lykova A.V., Pankov A.M., Ugolnikov M.V. Effect of Internal Technological Defects and Loading Waveform on Structural Composite Fatigue Life, Fract. Struct. Integr., 71 (2025) pp. 1-10. DOI: https://doi.org/10.3221/IGF-ESIS.71.01
[8] Zhou, J. (2024). Exploring shear nonlinearity of plain-woven composites at various temperatures based on machine learning, Compos. Struct.
[9] Barile, C., Casavola, C., Pappalettera, G., Paramsamy Kannan, V. (2022). Damage monitoring of carbon fibre reinforced polymer composites using acoustic emission technique and deep learning, Compos. Struct., 292, p. 115629. DOI: https://doi.org/10.1016/j.compstruct.2022.115629.
[10] Wang, Y., Chen, D., Li, N., Yuan, H., Zhu, Z., Li, Y., Huang, Z. (2020). A micromechanics based elasto-plastic damage model for unidirectional composites under off-axis tensile loads, Sci. Rep., 10(1), p. 847. DOI: https://doi.org/10.1038/s41598-020-57771-8.
[11] Behera, A., Thawre, M.M., Ballal, A. (2019). Failure Analysis of CFRP Multidirectional Laminates Using the Probabilistic Weibull Distribution Model under Static Loading, Fibers Polym., 20(11), pp. 2390–2399. DOI: https://doi.org/10.1007/s12221-019-1194-9.
[12] Chakrapani, S.K., Dayal, V. (2019). Destructive and Nondestructive Evaluation of Dry Spots in Thick Glass Fiber Reinforced Composites, Appl. Compos. Mater., 26(2), pp. 693–708. DOI: https://doi.org/10.1007/s10443-018-9744-7.
[13] Hamidi, Y.K., Altan, M.C. (2017). Process Induced Defects in Liquid Molding Processes of Composites, Int. Polym. Process., 32(5), pp. 527–544. DOI: https://doi.org/10.3139/217.3444.
[14] Han, K., Lee, L.J. (1996). Dry Spot Formation and Changes in Liquid Composite Molding: I—Experimental, J. Compos. Mater. DOI: https://doi.org/10.1177/002199839603001303.
[15] Fu, Y., Yao, X. (2022). A review on manufacturing defects and their detection of fiber reinforced resin matrix composites, Compos. Part C Open Access, 8, p. 100276. DOI: https://doi.org/10.1016/j.jcomc.2022.100276.
[16] Hamidi, Y.K., Aktas, L., Altan, M.C. (2008). Effect of Nanoclay Content on Void Morphology in Resin Transfer Molded Composites, J. Thermoplast. Compos. Mater. DOI: https://doi.org/10.1177/0892705707083635.
[17] LeBel, F., Ruiz, É., Trochu, F. (n.d.). Void content analysis and processing issues to minimize defects in liquid composite molding. DOI: https://doi.org/10.1002/pc.24609.
[18] Talreja, R. (2024). Failure Analysis of Composite Materials with Manufacturing Defects, Boca Raton, CRC Press, DOI: https://doi.org/10.1201/9781003225737.
[19] Chen, Y., Zhang, J., Li, Z., Zhang, H., Chen, J., Yang, W., Yu, T., Liu, W., Li, Y. (2023). Manufacturing Technology of Lightweight Fiber-Reinforced Composite Structures in Aerospace: Current Situation and toward Intellectualization, Aerospace, 10(3), p. 206. DOI: https://doi.org/10.3390/aerospace10030206.
[20] Sun, S., Han, Z., Fu, H., Jin, H., Dhupia, J.S., Wang, Y. (2020). Defect Characteristics and Online Detection Techniques During Manufacturing of FRPs Using Automated Fiber Placement: A Review, Polymers, 12(6), p. 1337. DOI: https://doi.org/10.3390/polym12061337.
[21] Strungar, E.M., Lobanov, D.S., Staroverov, O.A., Pelenev, K.A. (2025). Improvement of the method of digital image correlation in the field of analyzing the processes of deformation and fracture of composites, Ind. Lab. Diagn. Mater., 91(1), pp. 60–68. DOI: https://doi.org/10.26896/1028-6861-2025-91-1-60-68.
[22] Strungar, E., Lobanov, D., Chebotareva, E., Kochneva, Y. (2024). Mechanical behavior of fiber-glass plastic with hole pattern using digital image correlation and acoustic emission methods, Fract. Struct. Integr., 18(68), pp. 63–76. DOI: https://doi.org/10.3221/IGF-ESIS.68.04.
[23] Gao, Z., Zhang, Q., Su, Y., Wu, S. (2017). Accuracy evaluation of optical distortion calibration by digital image correlation, Opt. Lasers Eng., 98, pp. 143–152. DOI:https://doi.org/ 10.1016/j.optlaseng.2017.06.008.
[24] Pan, B. (2018). Digital image correlation for surface deformation measurement: historical developments, recent advances and future goals, Meas. Sci. Technol., 29(8), p. 082001. DOI: https://doi.org/10.1088/1361-6501/aac55b.
[25] Sutton, M.A., Orteu, J.-J., Schreier, H. (2009). Image Correlation for Shape, Motion and Deformation Measurements, Boston, MA, Springer US, DOI: https://doi.org/10.1007/978-0-387-78747-3.